Fast gas heating and kinetics of electronically excited states in a nanosecond capillary discharge in CO2

G V Pokrovskiy, N A Popov, S M Starikovskaia

Fast gas heating and kinetics of electronically excited states in a nanosecond capillary discharge in CO_2

G V Pokrovskiy[1], N A Popov[2] and S M Starikovskaia[1]

[1]Laboratoire de Physique des Plasmas, CNRS, Sorbonne Université, Université Paris-Saclay, École Polytechnique, Institut Polytechnique de Paris, F-91128, Palaiseau, France

[2]Skobel'tsyn Institute of Nuclear Physics, Moscow State University, Leninskie gory, Moscow 119991, Russia

E-mail: georgy.pokrovskiy.m1@polytechnique.edu
svetlana.starikovskaia@lpp.polytechnique.fr

November 2021

Abstract. Fast gas heating in a pulsed nanosecond capillary discharge in pure CO_2 under the conditions of high specific deposited energy (around 1.2 eV/molecule) and high reduced electric fields (150–250 Td) has been studied experimentally and numerically. Specific deposited energy, reduced electric field and gas temperature have been measured as functions of time. The radial distribution of the electron density has been analyzed experimentally. The role of quenching of $O(^1D)$, $O(^1S)$ and $CO(a^3\Pi)$ excited atoms and molecules leading to heat release at sub-microsecond time scale have been analyzed by numerical modeling in the framework of 1D axial approximation.

1. Introduction

1.1. General observations of plasma-assisted conversion of CO_2

Conversion of carbon dioxide by plasma is the object of scientific research since the second half of the XX century. Many scientific works are devoted to theoretical and experimental study of mechanisms of dissociation of CO_2. Dissociation of carbon dioxide in non-equilibrium plasma are described in [1–3] where various experiments with radio-frequency (RF) and microwave (MW) discharges with dominant role of vibrational excitation in CO_2 dissociation are mentioned. Along with this, a wide range of recent studies [4] on the problem of CO_2 conversion in gas discharges has confirmed the great interest in this problem. A number of experimental and computational studies have been devoted to CO_2 conversion in 'cold' plasma discharges, such as dielectric-barrier discharges, corona discharges, pulsed nanosecond discharges et al. In these discharges, the dominating channel of CO_2 conversion is usually the dissociation of mixture molecules by electron impact. A detailed review of the available electron impact cross-sections in CO_2 plasmas is given in [5]. The cross-sections reported by Phelps [6] are widely used in

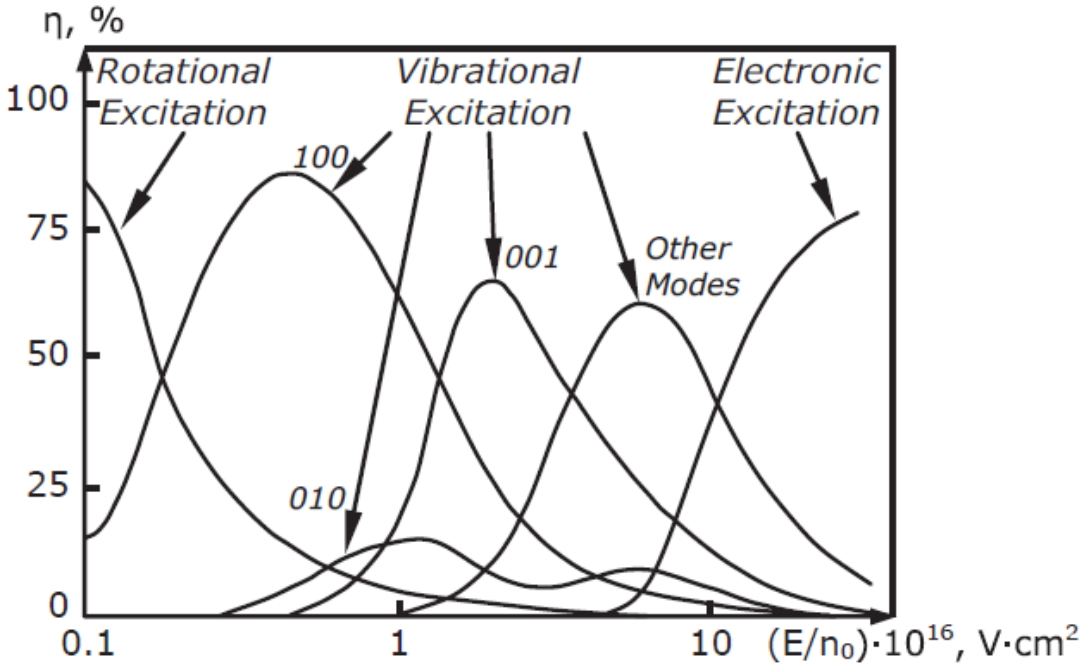

Figure 1. Fractions of discharge energy transferred from plasma electrons to different channels of CO_2 excitation; 1 Td corresponds to 10^{-17} V·cm^2. Taken from [1].

the literature. The set contains two electronic excitation cross-sections, with thresholds at 7 and 10.5 eV. The cross-sections calculated theoretically by Polak and Slovetsky [7] are described in [4] where the cross-sections of excitation of two electronic states of CO_2 by electronic impact are given as well. More recent publications [8, 9] justify the relevance of cross-sections given in [7] both by numerical modeling and experiment for values of the reduced electric field $<$ 100 Td. However, it has been shown in [10] that the set of cross-sections by Phelps [6] provide the best agreement with the set of experimental data of the CO_2 conversion efficiency in corona and dielectric-barrier discharges by electron impact for values of the reduced electric field $>$ 90 Td.

A number of publications on the domain were released in the last decade. Time- and space- resolved actinometry measurements of the dissociation fraction performed in a CO_2 microwave discharge are presented in [11]. Experiments on carbon dioxide dissociation in atmospheric pressure DBD discharge are described in [12]. A series of experiments with various input energies per particle (0.1 - 20 eV per molecule) has been done. The corresponding dissociation fraction ‡ was measured in gas exhaust by *ex-situ* FTIR-spectroscopy and was equal 0.1% - 4.4%. The energy efficiency of the process §

‡ $\alpha = \frac{[CO]}{[CO]+[CO_2]}$

§ Energy efficiency of CO_2 dissociation is defined as $\eta = \alpha E_{min}/w$, where α is dissociation fraction of CO_2, E_{min} = 2.93 eV is minimal energy value required for CO_2 splitting: $CO_2 \longrightarrow CO + 1/2\ O_2$, w (eV/molecule) is specific deposited energy.

remained below 5%. The dominant role of the vibrational excitation in carbon dioxide dissociation is underlined. The optical emission spectroscopy revealed molecular bands witnessing the presence of electronically excited states of CO_2^+. The presence of CO_2 dissociation via electronic excitation could be therefore confirmed. A detailed approach to studies of the role of vibrational excitation in plasma assisted conversion of CO_2 is given in 2017 [13]. The temperatures of different vibrational modes of CO_2 in a pulsed glow discharge at 6.7 mbar were measured as a function of time and a particular role of asymmetric mode has been reported. The rotational temperature directly after the voltage pulse was between 530 K and 860 K and the relaxation time of the rotational temperature was reported to be between 0.1 ms and 0.4 ms.

Theoretical background of the domain is represented by a thorough and detailed research. Detailed zero-dimensional kinetic models are described in [14–17]. A recent review [18] demonstrating the state-of-the-art of theoretical, modeling and experimental aspects of plasma assisted conversion has been released by a collaboration of several European scientific groups.

1.2. CO_2 dissociation in nanosecond discharges at high specific deposited energy

There are several recent publications concerning dissociation of carbon dioxide in nanosecond discharges. An experiment with nanosecond repetitive pulse (NRP) discharges in atmospheric pressure in pin-to-sphere configuration is described in [19]. LIF measurements of gas temperature showed that the gas is heated up to 2500 K for few μs after the first high voltage pulse. The maximal value of dissociation fraction was as high as 20% whereas the dissociation efficiency was equal to 12%, which corresponds to the energy cost $E_c \approx 24$ eV/molecule. In its turn, the energy efficiency reached the maximal value of 30% ($E_c \approx 10$ eV/molecule) whereas the dissociation fraction was equal to 14 %. The measurements were done in dry and humid CO_2. Other experiments with NRP discharge are described in [20–22]. The roles of cooled cathode and temporal configuration of the high voltage pulse are underlined. In particular, the influence of time between pulses T_p on the efficiency and conversion of carbon dioxide has been shown. The essential point of this effect is related to the fact that each new pulse comes to a perturbed plasma and 'memory effects' thus play an important role. It is therefore possible to control the energy efficiency and conversion degree by varying the time between pulses. Moreover, different regimes correspond to dominance of either vibrational or electronical mechanisms of CO_2 decomposition.

Paper [22] discusses temperature measurements on the basis of the rotational distribution of $N_2(C^3\Pi_u)$ when adding 5% of nitrogen to CO_2. Analysis of gas temperature measurements by the rotational distribution of $N_2(C^3\Pi_u)$ in CO_2:N_2 mixture is presented, but the possibility of an additional population of $N_2(C^3\Pi_u)$ by electron impact excitation from $N_2(A^3\Sigma_u^+)$ state in the discharges with high excitation degree was not

taken into account.

The dissociation of CO_2 via electronic degrees of freedom becomes the dominant mechanism of dissociation at the values of reduced electric field E/n of hundreds of Td (see Figure 1). One of the ways of creation of such strong reduced electric fields is to produce a high-voltage discharge, initiated by a fast ionization wave at moderate pressures [23, 24]. Therefore, a nanosecond capillary discharge ignited in pure carbon dioxide at moderate (10-20 mbar) pressures described in the current paper seems to be an efficient plasma source with relatively high values of specific deposited energy and reduced electric field.

One of the important signatures of a nanosecond capillary discharge is high values of dissociation degree of mixture molecules. For instance, the dissociation fraction of oxygen molecules in such a discharge ignited in air was very close to 100 % [25, 26]. TALIF measurements of a nanosecond discharge conducted on the same setup in pure nitrogen have revealed a dissociation fraction of 10 % at 1 ms after the fast ionization wave had passed [27].

Nanosecond capillary discharges at high reduced electric fields and high specific deposited energy are unique not only because they make high values of dissociation degree possible but for the reasons of the so-called phenomenon of fast gas heating (FGH) [28, 29]. Nanosecond discharges are characterized by relatively high values of reduced electric field, thereby a significant part of discharge energy goes to electronic excitation of species. Quenching of the electronically excited states defines the release of the energy to translational degrees of freedom. The previous studies of the FGH in nanosecond discharges in N_2:O_2 mixtures [24, 25, 30, 31] have demonstrated that specific deposited energy at reduced electric field of 100-400 Td may exceed 1 eV/particle and the fraction of discharge energy spent to the gas heating could reach 20-30 %.

The main objects of the study described in the current paper are the role of the electronic excitation in fast gas heating of CO_2 at high values of reduced electric field and the role of atomic species in the radial distribution of electron densities and ion composition in the discharge at high values of specific deposited energy.

2. Experimental procedure

2.1. General remarks

The general scheme of the experimental setup and the main experimental equipment are presented in Figure 2. The triggering generator (TG) BNC 575 was used to trigger the high voltage generator (HVG) FPG 12-1NM (FID GmbH) and the ICCD camera. The voltage amplitude of the positive polarity pulse provided by the HVG during the

experiment was equal to 9.4 kV, the width of the pulse was 30 ns FWHM and the rise time was 2 ns. It is important to notice that a high voltage pulse sent from the HVG was partially reflected from the discharge cell because of the mismatching of the cable and the discharge cell and then propagated back and forth between HVG and the discharge cell forming 3 consequent pulses in the latter. The amplitudes of the further pulses were negligible with respect to the first 3 pulses.

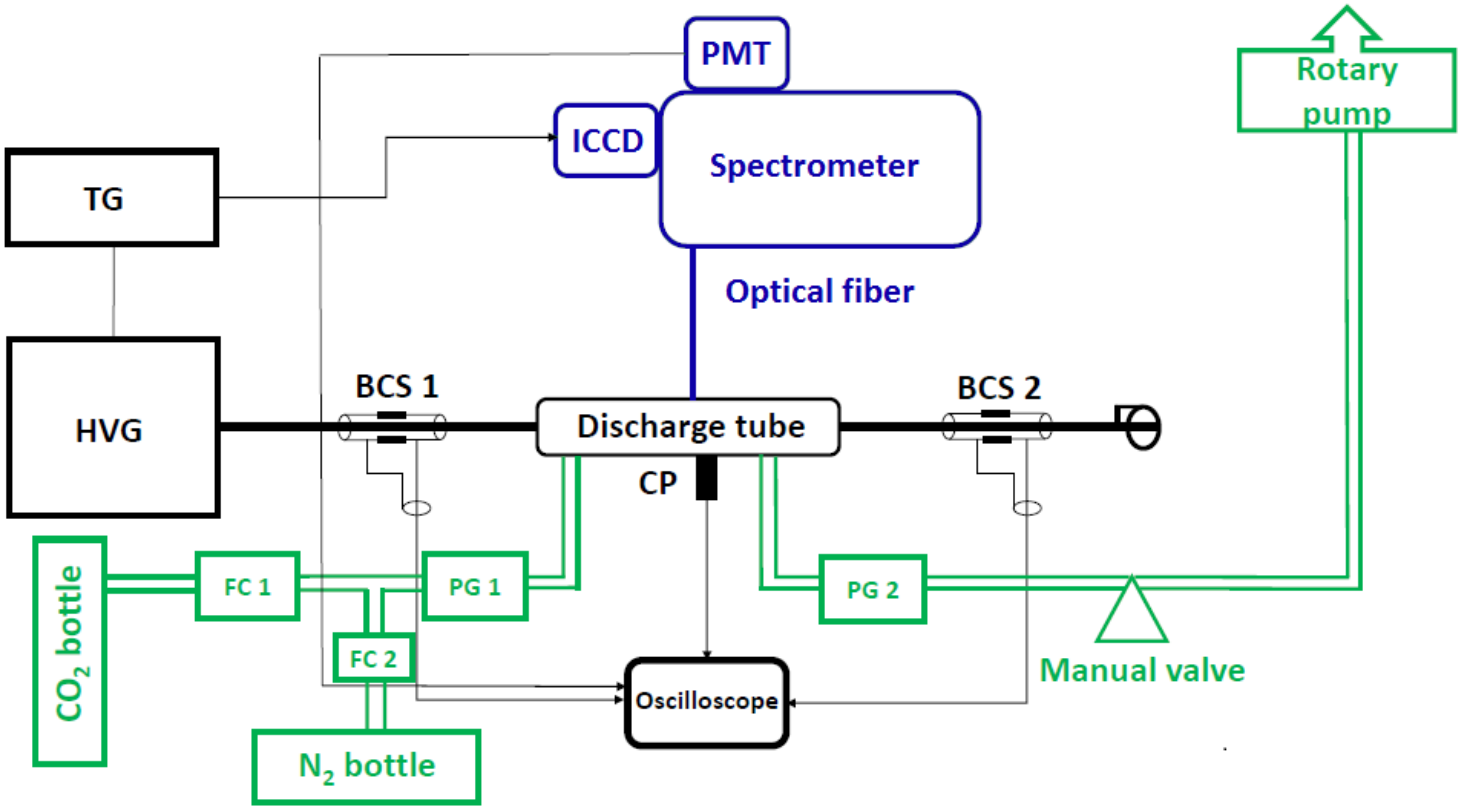

Figure 2. Scheme of the experimental setup. FC1 and FC2 are mass flow controllers, PG1 and PG2 are pressure gauges, BCS is back current shunt, CP is capacitive probe. PMT is photomultiplier tube, TG is triggering generator, HVG is high voltage generator. Black color designates electrical supplies, green color designates vacuum system and system of gas flow control, blue color designates optical system.

The setup was operating at pressures of 19.4 mbar at flow values of 10-11 sccm. CO_2 and N_2 (the latter was used only when gas temperature was being measured) flow was controlled by Brooks Instruments 5850TR mass flow controllers operated from Brooks Instruments Model 0254 control panel. The pressure in the system was measured by two pressure gauges Pfeiffer Vacuum CMR 362 installed by two opposite sides of the discharge cell. The mean value of their data was considered to be the real pressure.

The scheme of the discharge cell is presented in the Figure 3. The discharge cell was installed in the break of the high voltage cable. The capillary with two brass electrodes

was made from quartz. The distance between the electrodes of 75 mm. The length of the capillary was equal to 86 mm. The internal and external diameters of the capillary were equal to 1.5 mm and 3.0 mm, respectively. The rectangular (48 mm x 60 mm) metal screen surrounding the capillary tube was connected to the shielding of both HV and LV cables. Such configuration made possible measurements of the temporal profile of the electric field by a capacitive probe. Capacitive probe is a custom-made calibrated charge detector, the details of the electric field measurements are described in [23]. The applied voltage, electric current flowing through plasma as well as deposited energy were measured by two custom-made calibrated back current shunts (BCS1 and BCS2) installed on HV and LV cables, respectively. The details of the procedure can be found in [32] and will be briefly described below.

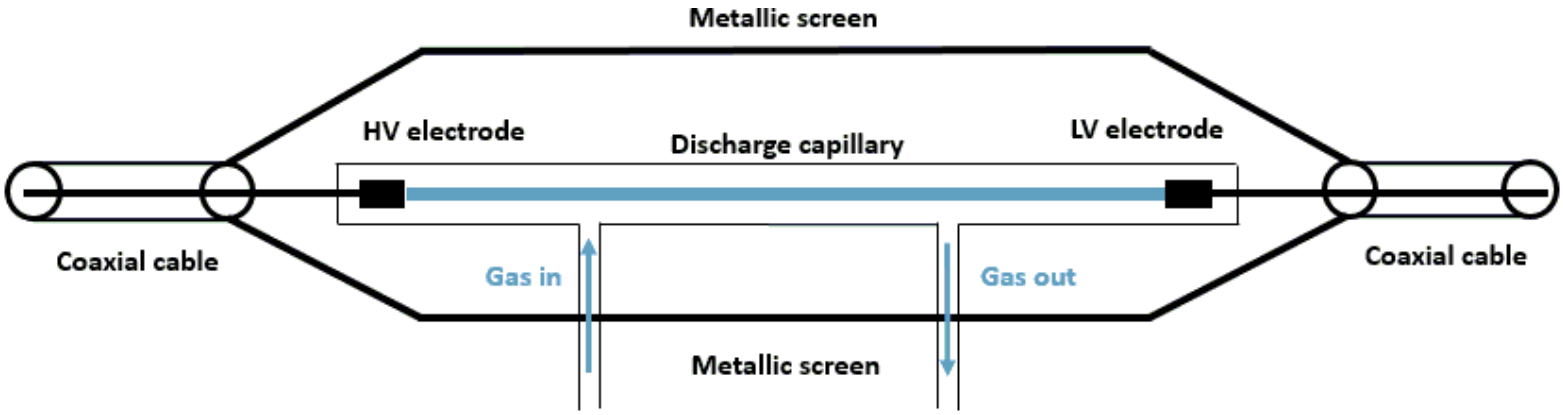

Figure 3. Scheme of the discharge cell consisting of the capillary and the metallic screen

2.2. Temperature measurements

To measure the gas temperature, 1 sccm of nitrogen admixture was added to 10 sccm of pure CO_2. The emission spectra were acquired by the combination of the Princeton Instruments spectrometer Acton Series SP-2500i with the ICCD camera (PI-MAX 4 1024i, Princeton Instruments). The gate of the camera was equal to 10 ns and the camera acquired the signal with different delays relative to the start of the first discharge pulse. The rotational temperature of $N_2(C^3\Pi_u)$ was then derived from the $0 \rightarrow 0$ vibrational transition of the second positive system (SPS, 337 nm), description of this technique can be found elsewhere [33]. The rotational temperature of the $N_2(C^3\Pi_u)$ state was fitted using the SpecAir [34] software.

To check how the additions of N_2 influence the discharge in CO_2, a set of experiments where percentage of N_2 was changed between 9% and 33% was performed. Although intensities of molecular bands were different, similar deposited energies, electric fields and rotational distributions in OES spectra were obtained for different percentage of N_2.

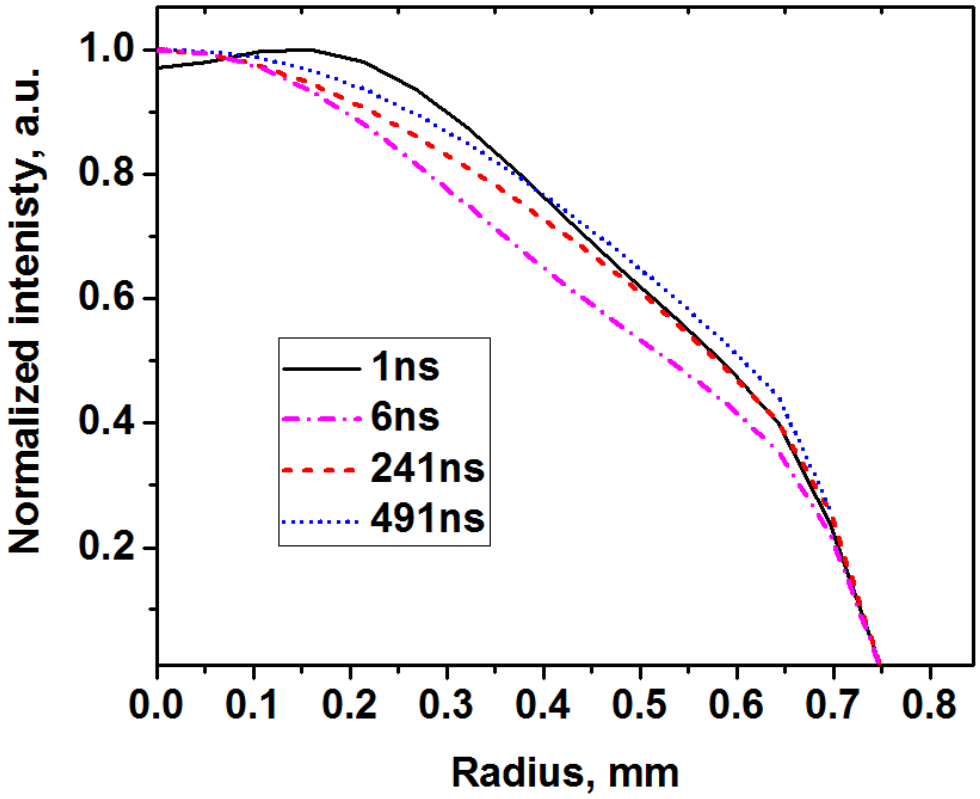

Figure 4. Normalized experimental radial profiles of the emission of $N_2(C^3\Pi_u)$ at different time instants. Solid black curve: 1 ns, first pulse; magenta dashed dot curve: 6 ns, first pulse; dashed red curve: 241 ns, second pulse; blue dotted curve: 491 ns, third pulse.

It was concluded that, for given parameters, the presence of N_2 influenced the chemistry of plasma but did not influenced the electron kinetics and the gas temperature.
It is important that such a technique of measurements of the gas temperature is only valid if the $N_2(C^3\Pi_u)$ is populated by electron impact directly from the ground $N_2(X^1\Sigma_g^+)$ state and population of the $N_2(C^3\Pi_u)$ from intermediate $N_2(A^3\Sigma_u^+)$ and $N_2(B^3\Pi_g)$ states is negligible. A justification of this fact will be presented in the Discussion part.

2.3. Measurements of the radial profile of SPS radiation intensity

To conduct the measurements of radial distribution of the emission intensity, the ICCD camera was used. The camera was installed 30 cm away from the capillary such that the beams coming from the capillary could be treated as parallel ones. The camera captured the beams from the central part of the capillary. Therefore, a profile of emission intensity with respect to the vertical (perpendicular to the axis of the capillary) coordinate was obtained. The profiles were taken in CO_2:N_2 = 10:1 mixture with a narrow ($\Delta\lambda$ = 5 nm) bandpass filter with the central wavelength λ = 380 nm. Again, the

Table 1. Main discharge characteristics in all three pulses

Number of pulse	1	2	3
Peak current, A	58	66	26
w, eV/particle	0.42	0.6	0.2
Peak n_e, $10^{15} \cdot \mathrm{cm}^{-3}$	0.95	1.14	0.5
Temperature, K	350-600	800	1100

emission of the SPS was studied. The profiles were taken at different time instants in all three high voltage pulses (Figure 4). The gate of the camera was equal to 3 ns. According to the assumption of cylindrical symmetry of the emission intensity, the procedure of numerical inverse Abel transform was applied to experimental profiles. The emission of quartz was subtracted in order to separate the signal coming from the internal part of the capillary similar to procedure presented in [31].

The radial profile of radiation intensity of the second positive system of nitrogen is related to the radial profile of the electron density provided that two conditions are met. First, the emitting $N_2(C^3\Pi_u)$ state should be populated by electron impact from the ground state $N_2(X^1\Sigma_g^+)$ (the verification of the condition will be presented in the Discussion part). Second, the quenching rate of $N_2(C^3\Pi_u)$ should be independent on the radial coordinate. Under given conditions $N_2(C^3\Pi_u)$ state is mainly quenched by CO_2 molecules. The rate constant of this process is relatively high and equal to $k_q = 3 \cdot 10^{-10}$ cm^3/s [35], therefore this process is dominant and the second condition is fulfilled.

Will note that a typical radial size of the gas heating region at the given conditions is close to $R_h = 0.6$ mm. The characteristic time of gas expansion in radial direction τ_g is determined by the sound speed C_s in the heated gas: $\tau_g = R_h/C_s \approx 1.5$ μs. Since the time delay between the consequent pulses is equal to 240 ns, it can be concluded that the gas density does not significantly change before the end of the third pulse. This fact will be used in following data treatment.

2.4. Electric characteristics of the discharge

The experimental results of measurements of the electric current transmitted through the discharge cell and reduced electric field in all three high voltage pulses are given in the Figure 5. The electric current has been recorded by the BCS2 and the reduced electric field has been recorded by the capacitive probe. The details of the corresponding methods can be found elsewhere [23]. It can be seen that the first pulse is characterized by the propagation of the fast ionization wave from the high voltage electrode to the low voltage one (from -20 to 0 ns). As soon as the fast ionization wave reaches the low voltage electrode, the low voltage cable is charged and the conduction current starts to flow.

The main discharge characteristics such as peak electric current, specific deposited energy w and the peak electron density n_e are presented in the Table 1. The specific deposited energy has been calculated in the following way:

$$w(t) = \frac{\int_0^t \left(U_{inc}(t')^2 - U_{ref}(t')^2 - U_{tra}(t')^2\right)dt'}{ZN},$$

where $U_{inc}(t)$ is a waveform of incident voltage (recorded by BCS1, $U_{ref}(t)$ is a waveform of the voltage reflected from the discharge cell (recorded by BCS1) and $U_{tra}(t)$ is a waveform of the voltage transmitted through plasma (recorded by BCS2); N is the total number of particles in the discharge, Z=50 Ohm is the wave resistance of the cable.

The temporal profile of the electron density could be obtained according to the following considerations. The electric current flowing in the discharge can be expressed in a following way:

$$I(t) = en_e(t)v_{dr}(t)S,$$

where e is elementary charge, S is the cross-section of the discharge capillary $v_{dr}(t)$ is the drift velocity which can be calculated as a function of the reduced electric field using the BOLSIG+ [36] code. Therefore the electron density $n_e(t)$ could be derived.

2.5. Accuracy of measurements

The experiments presented in the present work include study of (i) radial distribution of emission intensity, (ii) electric current and electric field, (iii) specific deposited energy and (iv) gas temperature, all the data were acquired as function of time. The temporal resolution of the electric signals was defined by bandwidth of the back current shunts and the capacitive probe equal to 1 ns and 0.5 ns, respectively. Temporal resolution of optical emission spectroscopy was limited by the gate of the ICCD camera, the minimum possible gate was equal to 0.5 ns. Then, the accuracy of the synchronization of waveforms of the electric current and voltage was limited by sampling frequency of the oscilloscope and was equal to $\pm$0.2 ns. The details of the synchronization process are given in [23]. Relative error of measurements of current and voltage did not exceed several percent, relative error of measurements of specific deposited energy was not higher than 10% and the absolute error of temperature measurements was $\pm$50 K.

3. Description of the kinetic model

The numerical modeling focuses on the detailed kinetics in CO_2 plasma after closing of the discharge gap by FIW and in the near afterglow. The initial electron density distribution, $n_e(r)$, and the waveform of the conductive current both analyzed experimentally, were taken as the input data of the code.

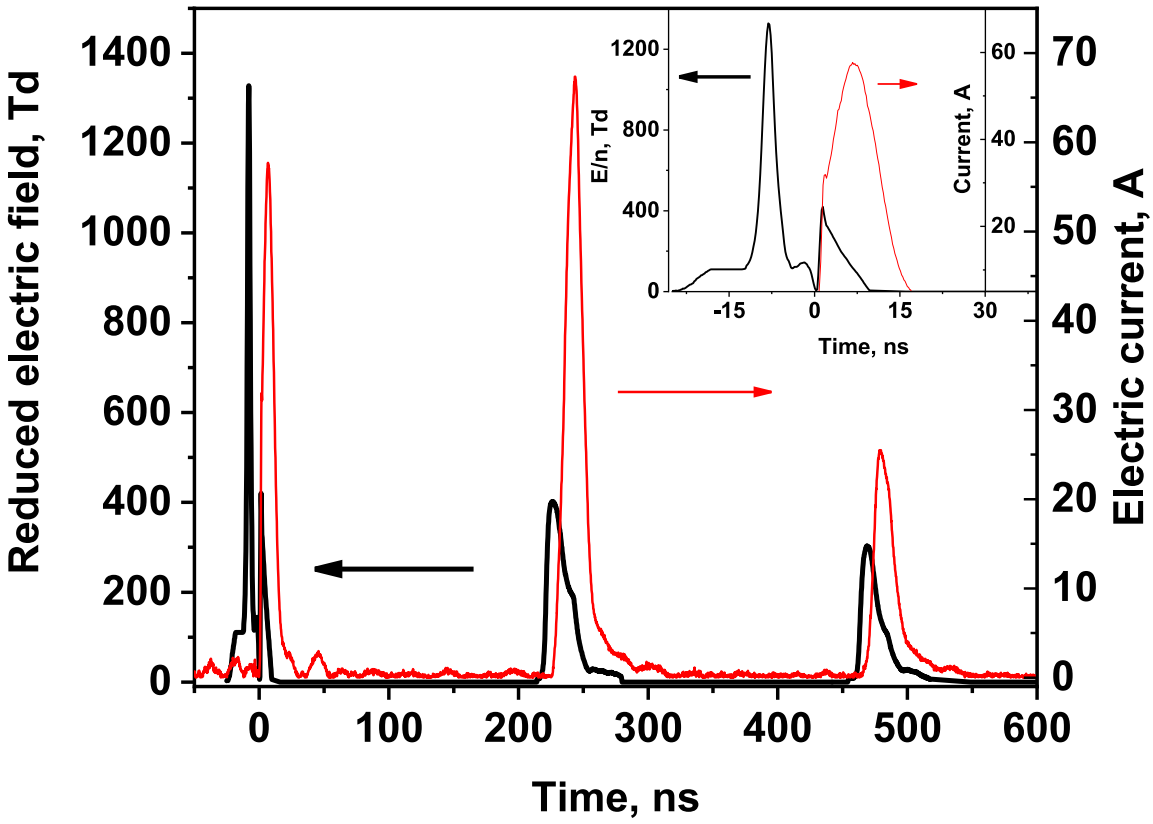

Figure 5. Waveforms of the reduced electric field (Td) and electric current (A). High-voltage pulses start at time instants −25 ns, 215 ns and 455 ns. The time instant t=0 in time axis is referred to the beginning of flowing of the conduction current in the discharge cell. The insert represents a zoom on the reduced electric field and electric current in the first pulse.

The calculations were carried out in 1-D approximation describing the particle density as function of radius r over the cross-section of measurements at axial symmetry. The validity of suggested approximation is proved by the fact that radial gradients of the discharge parameters are much higher than the axial gradients in the direction between the electrodes. The longitudinal electric field E and the specific deposited energy $\omega(r,t)$ in the discharge were calculated as:

$$E(t) = \frac{I(t)}{2\pi e \int_0^R n_e(r,t)\mu(r,t) r dr}; \qquad \omega(r,t) = \frac{1}{n}\int_0^t j_e(r,\tau)E(\tau)d\tau, \qquad (1)$$

where $n_e(r)$ is the radial electron density profile, $\mu(r)$ is the radial profile of the electron mobility, which depends on E/n, $R = 0.75$ mm is internal radius of the discharge tube, n is the gas density and j_e is the current density in the discharge.

To verify the results of the calculation, the experimentally measured reduced electric field was compared with $E(t)/n$ dependence calculated from the equation (1).

The following kinetic equation was being solved to calculate the electron density:

$$\frac{\partial n_e}{\partial t} = \frac{1}{r}\frac{\partial}{\partial r}\left(rD_a\frac{\partial n_e}{\partial r}\right) + n_e(\nu_i - \nu_a) - Q_r + Q_d \tag{2}$$

here, D_a is the ambipolar diffusion coefficient; ν_i and ν_a are the electron impact ionization and attachment frequencies; Q_r is the electron-ion recombination rate; the term Q_d accounts for all the processes of electron detachment from negative ions in collisions with $O(^3P)$ atoms, CO molecules, etc. The densities of other charged species are determined from similar balance equations.

Ionization and excitation rates were calculated for each time instant as a function of reduced electric field on the basis of the solution of the Boltzmann equation in a two-term approximation using BOLSIG+ code [36] with the imported cross-sections [6]. The set of cross-sections contains two electronic excitation cross-sections with thresholds 7 eV and 10.5 eV, which correspond to two dissociation channels giving $CO(X^1\Sigma^+) + O(^1D)$ and $CO(a^3\Pi_r) + O(^3P)$. In [10] the authors considered the regimes in which CO_2 conversion proceeds mainly due to the electron impact dissociation of CO_2 molecules. It is shown that the best fit with the set of experimental data of the conversion efficiency in the corona and dielectric-barrier discharges is provided by using, as the dissociation cross-section, of the cross-section by Phelps [6], for excitation of electronic states with the energy threshold of 10.5 eV.

The electron energy distribution function and hence the rate constants of electronic excitation, dissociation, and ionization of molecules by electron impact in vibrationally excited CO_2 depend, besides E/n, on the vibrational temperature of molecules. This effect can be approximately taken into account using the multiplying factor F [17], depending on the vibrational temperature T_v as:

$$F = exp\left(\frac{C_v z_v}{(E/n)^2}\right), \qquad z_v = exp\left(-\frac{E_v}{kT_v}\right) \tag{3}$$

here $E_v = 0.29$ eV is the quantum of asymmetric vibrational mode of CO_2, and $C_v = 7 \cdot 10^3$ Td^2 [17]. In the considered range of discharge parameters, $E/n = 200$ Td, $T_v \leq 4000$ K, the factor F does not exceed 1.08, so the effect of the vibrational temperature on the rate constants can be neglected.

The following main species were considered by the model for CO_2 plasma: CO_2, $CO(X^1\Sigma^+)$, $CO(a^3\Pi_r)$, $O_2(X^3\Sigma_g^-)$, $O(^3P)$, $O(^1D)$, $O(^1S)$, e, CO_2^+, CO_4^+, $C_2O_3^+$, $C_2O_4^+$, O_2^+. Hereinafter, the $CO(X^1\Sigma^+)$ species will be designated as CO. Along with that, the reactions involving nitrogen species, $N_2(X^1\Sigma_g^+)$, $N_2(A^3\Sigma_u^+)$, $N_2(B^3\Pi_g)$, $N_2(C^3\Pi_u)$,

$N_2(a'^1\Sigma_u^-)$, N_2^+, N_4^+, were taken into account for description of the temporal dynamics of the SPS radiation. The main reactions influencing the fast gas heating and/or the radial discharge structure and their rate constants are presented in Table 2.

The experiments made it clear that CO_2 is rapidly heated by high-power discharges. The dynamics of the gas temperature in the model was described by the equation [28]:

$$nC_V\frac{\partial T}{\partial t} = \frac{1}{r}\frac{\partial}{\partial r}\left(r\lambda\frac{\partial T}{\partial r}\right) + \frac{\varepsilon_v(T_v) - \varepsilon_v(T)}{\tau_{VT}} + W_R, \tag{4}$$

where C_V is the specific heat capacity of CO_2 at constant volume, $\lambda(T)$ is the thermal conductivity, ε_v is the mean vibrational energy per CO_2 molecule, τ_{VT} is the characteristic time of the VT – relaxation of CO_2(v) and W_R is the gas heating rate in chemical reactions.

To describe the mechanism of fast gas heating, energy branching in each exothermic reaction was studied. The energy delivered into translational degrees of freedom could be therefore found by taking into account the energy defect ΔE of the reactions.

(i) The reaction:

$$CO(a^3\Pi) + CO \longrightarrow CO(v) + CO(v) \tag{R7}$$

has been studied in [37]. It has been shown that approximately 90% of energy of $CO(a^3\Pi)$ comes to the vibrational excitation of the reaction products. Consequently, the energy spent to the fast gas heating was assumed to be equal to 0.6 eV. The same assumption has been applied to the reaction (R6).

(ii) It has been shown in [38] that the main products of quenching of $N_2(A^3\Sigma_u^+)$ molecules by atomic oxygen are excited $O(^1S)$ atoms:

$$N_2(A^3\Sigma_u^+, v{=}0{,}1) + O(^3P) \longrightarrow N_2(X^1\Sigma_g^+) + O(^1S). \tag{5}$$

One can notice that the values of excitation energy of $N_2(A^3\Sigma_u^+)$ and $CO(a^3\Pi)$ are close to each other and equal to 6.17 eV and 6.0 eV [39], respectively. Therefore, it could be assumed that quenching of $CO(a^3\Pi)$ leads to the formation of $O(^1S)$ atoms as well:

$$CO(a^3\Pi, v{=}0{,}1) + O(^3P) \longrightarrow\ CO(v{=}0{,}1) + O(^1S). \tag{R8}$$

The energy defect (ΔE $\approx$ 1.8 eV) comes to the gas heating.

(iii) Collisions of $O(^1S)$ and $O(^3P)$ atoms leads to the formation of an excited O_2^* molecule with excitation threshold of 9.3 eV. The term of the O_2^* electronic state intersects with the $O_2(B^3\Sigma_u^-)$ repulsive term which, in its turn, dissociates onto

Table 2. The main reactions used in the model

№	Process	Rate constant	Ref	ΔE, eV	Notes
R1	$CO_2 + e \longrightarrow CO_2^+ + 2e$	$f(E/n)$			
R2	$CO_2 + e \longrightarrow CO + O(^1D) + e$	$f(E/n)$			
R3	$CO_2 + e \longrightarrow CO(a^3\Pi) + O(^3P) + e$	$f(E/n)$			
R4	$CO + e \longrightarrow CO(a^3\Pi_r) + e$	$f(E/n)$			
R5	$CO(a^3\Pi_r) + CO_2 \longrightarrow 2{\cdot}CO + O(^3P)$	$5.0 \cdot 10^{-12}$ cm^3/s	[42]	0.55	
R6	$CO(a^3\Pi_r) + CO_2 \longrightarrow CO(v) + CO_2(v)$	$5.0 \cdot 10^{-12}$ cm^3/s	[42]	0.6	(i)
R7	$CO(a^3\Pi_r) + CO \longrightarrow CO(v) + CO(v)$	$5.7 \cdot 10^{-11}$ cm^3/s	[43]	0.6	(i)
R8	$CO(a^3\Pi_r) + O(^3P) \longrightarrow CO(v) + O(^1S)$	$1.9 \cdot 10^{-10}$ cm^3/s	[42, 43]	1.8	(ii)
R9	$O(^1S) + CO_2 \longrightarrow O(^1D) + CO_2(v)$	$4.0 \cdot 10^{-13}$ cm^3/s	[44]	1.33	
R10	$O(^1S) + CO \longrightarrow O(^1D) + CO(v)$	$1.0 \cdot 10^{-13}$ cm^3/s	[44]	1.33	
R11	$O(^1S) + O(^3P) \longrightarrow O(^1D) + O(^3P)$	$5.0 \cdot 10^{-11}\cdot \exp(-301/T_g)$ cm^3/s	[45]	2.23	(iii)
R12	$O(^1D) + CO_2 \longrightarrow O(^3P) + CO_2(v)$	$7.4 \cdot 10^{-11}\cdot \exp(133/T_g)$ cm^3/s	[46]	1.1	(iv)
R13	$O(^1D) + CO \longrightarrow O(^3P) + CO(v)$	$8.0 \cdot 10^{-11}$ cm^3/s	[44]	1.18	(v)
R14	$CO_2^+ + e \longrightarrow CO + O(^1D, {}^1S)$	$4.2 \cdot 10^{-7}\cdot (300/T_e)^{0.75}$ cm^3/s	[47]	6.4	
R15	$CO_2^+ + O(^3P) \longrightarrow O_2^+ + CO$	$2.5 \cdot 10^{-10}$ cm^3/s	[16]	1.0	
R16	$O_2^+ + e \longrightarrow O(^3P) + O(^3P, {}^1D)$	$2.0 \cdot 10^{-7}\cdot (300/T_e)^{0.7}$ cm^3/s	[47, 48]	5.0	
R17	$CO_2^+ + CO_2 + M \longrightarrow C_2O_4^+ + M$	$3.0 \cdot 10^{-28}\cdot (300/T_g)^{1.7}$ cm^6/s	[16]		
R18	$C_2O_4^+ + M \longrightarrow CO_2^+ + CO_2 + M$	(3-6) $\cdot 10^{-14}$ cm^3/s	[16]		
R19	$C_2O_4^+ + e \longrightarrow CO + O(^1D, {}^1S) + CO_2$	$1.9 \cdot 10^{-6}\cdot (300/T_e)^{0.33}$ cm^3/s	[47]	5.7	(vi)
R20	$C_2O_3^+ + e \longrightarrow$ *product*	$1.9 \cdot 10^{-6}\cdot (300/T_e)^{0.33}$ cm^3/s	[47]		
R21	$O_2^+ + CO_2 + M \longrightarrow CO_4^+ + M$	$5.0 \cdot 10^{-31}$ cm^6/s	[44]		

$O(^3P)$+$O(^1D)$. The energy defect is therefore spent to the gas heating.

(iv) It has been demonstrated in [40] that about 44% of excitation energy of $O(^1D)$ is delivered to vibrational excitation of CO_2 during the reaction:

$$O(^1D) + CO_2 \longrightarrow O(^3P) + CO_2(v). \quad \text{(R12)}$$

It has been therefore concluded that the percentage of $O(^1D)$ energy coming to FGH is equal to 56%. Thus, the energy spent to the fast gas heating in the reaction (R12) was assumed to be equal to 1.1 eV.

(v) Vibrational excitation of CO in reaction (R13):

$$O(^1D) + CO \longrightarrow O(^3P) + CO(v). \quad \text{(R13)}$$

has been studied in [41]. It has been shown that the part of excitation energy of $O(^1D)$ coming to vibrational excitation of CO doesn't exceed 40 %. According to that, the

fraction of energy coming to FGH is 60 % which is equal to 1.18 eV.

(vi) The rate constant of the reaction (R19) was assumed to be equal to the constant of the reaction (R20) whose products are assumed to be the same as during the recombination of CO_2^+ ion [49].

4. Results and discussion

4.1. Validity of the approach to measurements of gas temperature

As the gas temperature has been measured by the SPS of N_2 in a CO_2:N_2 = 10:1 mixture, it is necessary to show the correctness of these kinds of measurements. Rota-tional relaxation of $N_2(C^3\Pi_u)$ in nitrogen at $T > 300$ K demands at least 5 collisions [50, 51]. At this, according to [35], the cross-section of $N_2(C^3\Pi_u)$ state quenching by CO_2 molecules is close to the gas-kinetic cross-section. Thus, in CO_2:N_2 = 10:1 mixture $N_2(C^3\Pi_u)$ quenching is faster than the rotational relaxation (or "thermalisation") of this state. To be sure that the rotational temperature of $N_2(C^3\Pi_u)$ "copies" [24] the rota-tional temperature of the ground state of nitrogen, it was essential to verify that the only way of population of $N_2(C^3\Pi_u)$ was direct electron impact from the ground state and the rates of other reactions were negligible.

(i) Estimation of the role of pooling reaction (6):

$$N_2(A^3\Sigma_u^+) + N_2(A^3\Sigma_u^+) \longrightarrow N_2(C^3\Pi_u) + N_2(X^1\Sigma_g^+) \quad (6)$$

The time-resolved measurements of the intensity of emission of the second positive system at 337 nm by a photomultiplier tube (PMT) have shown that emission between the high voltage pulses is at zero level. Therefore, the only way of $N_2(C^3\Pi_u)$ population is electron impact.

(ii) If the electron density in pulses is high enough, an additional population of $N_2(C^3\Pi_u)$ by direct electron impact from excited electronic states $N_2(A^3\Sigma_u^+, B^3\Pi_g)$ [27] is possible:

$$N_2(A^3\Sigma_u^+, B^3\Pi_g) + e \longrightarrow N_2(C^3\Pi_u) + e. \quad (7)$$

Let us estimate the probability that the population of electronic states $N_2(A^3\Sigma_u^+, B^3\Pi_g)$ is so high that the reaction (7) becomes important. According to [52], the rate of the reaction

$$N_2(B^3\Pi_g) + CO_2 \longrightarrow N_2(X^1\Sigma_g^+) + CO + O \quad (8)$$

is $k^B_{CO_2} = 1.5 \cdot 10^{-10}$ cm^3/s. The main yield of the reaction (8) is dissociation of CO_2 molecules and not the population of electronic state $N_2(A^3\Sigma_u^+)$. Therefore, the population of $N_2(A^3\Sigma_u^+)$ does occur only by electron impact excitation of the $N_2(X^1\Sigma_g^+)$

Table 3. Comparison of experimental and calculated values of the specific deposited energy in all three high voltage pulses

Number of pulse	1	2	3
w (exp/calc), eV/particle	0.42/0.41	0.6/0.55	0.2/0.23

and quenching of $N_2(B^3\Pi_g, C^3\Pi_u)$ doesn't contribute significantly to the population of $N_2(A^3\Sigma_u^+)$. The ratio of the rate constants of electron impact excitation of $N_2(C^3\Pi_u)$ from $N_2(A^3\Sigma_u^+)$ and $N_2(X^1\Sigma_g^+)$ states is approximately equal to 50:1 at the E/n = 150-250 Td. In the current case when CO_2:N_2 = 10:1 and E/n = 150-250 Td the role of the reaction (7) becomes important only at $[N_2(A^3\Sigma_u^+)]$:$[N_2(X^1\Sigma_g^+)] > 2\%$. In our conditions of high values of specific deposited energy, the main factor responsible for the determination of $N_2(A^3\Sigma_u^+)$ density is fast quenching of this state by electrons leading to its dissociation [27]. The rate constant of $N_2(A^3\Sigma_u^+)$ dissociation at E/n = 150-250 Td is $k_q = (5\text{-}10) \cdot 10^{-8}$ cm^3 [27]. Given that the electron density in the 1st and the 2nd high voltage pulses is $n_e \approx 10^{15}$ cm^{-3} one obtains frequency of $N_2(A^3\Sigma_u^+)$ quenching ν_q = (5-10) $\cdot 10^7$ s^{-1}. Such a value is much higher than frequency of $N_2(A^3\Sigma_u^+)$ quenching via other channels. The rate constant k_{ex}^A of electron impact excitation of $N_2(A^3\Sigma_u^+)$ from the ground state of nitrogen:

$$N_2(X^1\Sigma_g^+) + e \longrightarrow N_2(A^3\Sigma_u^+) + e \tag{9}$$

is $k_{ex}^A = (1.1\text{-}1.5) \cdot 10^{-10}$ cm^3/s at E/n = 150-250 Td (calculated by BOLSIG+ solver [36] with the cross-sections imported from [6] and [53]. Thus, $[N_2(A^3\Sigma_u^+)]/[N_2(X^1\Sigma_g^+)] = k_{ex}^A/k_q$ = 0.2-0.3 %. As the ratio of the rate constants of excitation of $N_2(C^3\Pi_u)$ by electron impact from $N_2(A^3\Sigma_u^+)$ and $N_2(X^1\Sigma_g^+)$ states is approximately equal to 50:1 at E/n = 150-250 Td, one can conclude that the contribution of the population of $N_2(C^3\Pi_u)$ state by electron impact from $N_2(A^3\Sigma_u^+)$ state doesn't exceed 15 %. Therefore, the definition of gas temperature by the SPS of N_2 in a CO_2: N_2 = 10:1 mixture is justified.

4.2. Electric characteristics

As it has been mentioned previously, the waveforms of the electric current obtained in the experiments have been used as input data of the kinetic model (see Figure 2 and Table 1). A comparison of the calculated and experimental values of specific deposited energy at p = 19.4 mbar and T = 300 K is given in Table 3. The calculated values were averaged on the cross-section of the discharge tube.

Figure 6 represents both calculated and measured temporal dynamics of the reduced electric field E/n and calculated specific deposited energy at the tube axis (w_{axial}) and averaged on the tube cross-section ($w_{average}$) in the first pulse. The point is the measured value of the specific deposited energy averaged on the tube cross-section in the first pulse. Several important features should be noticed:

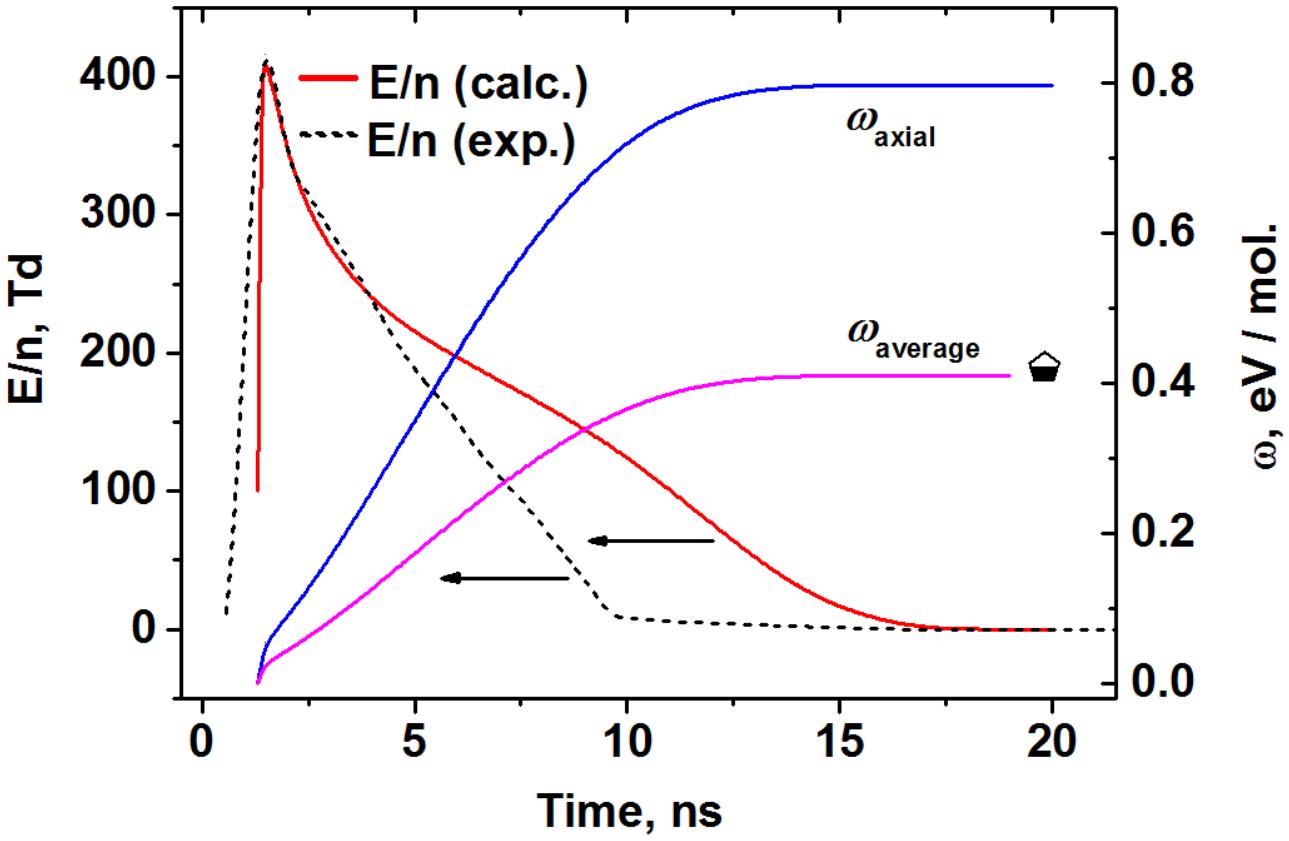

Figure 6. Temporal dynamics of the reduced electric field (solid red curve: calculations, dashed black curve: experiments). The data are given for the first high voltage pulse. Solid blue curve: calculated specific deposited energy at the tube axis. Solid magenta curve: calculated specific deposited energy averaged on the cross-section of the tube. The experimental point at 20 ns is given.

(i) The most part of energy is deposited at E/n = 150-250 Td. Thus, a significant value of dissociation degree of CO_2 might be observed and the phenomenon of fast gas heating might take place.

(ii) Specific deposited energy at the axis of the discharge tube (w_{axial}) is almost two times higher than the average value of the specific deposited energy ($w_{average}$). This fact is related to peculiarities of the initial distribution of the electron density (see Figure 4 and discussion in section 2.3).

(iii) The values of the specific deposited energy are particularly elevated at the axial part of the discharge cell ($w_{axial} > 2$ eV/particle during three high voltage pulses).

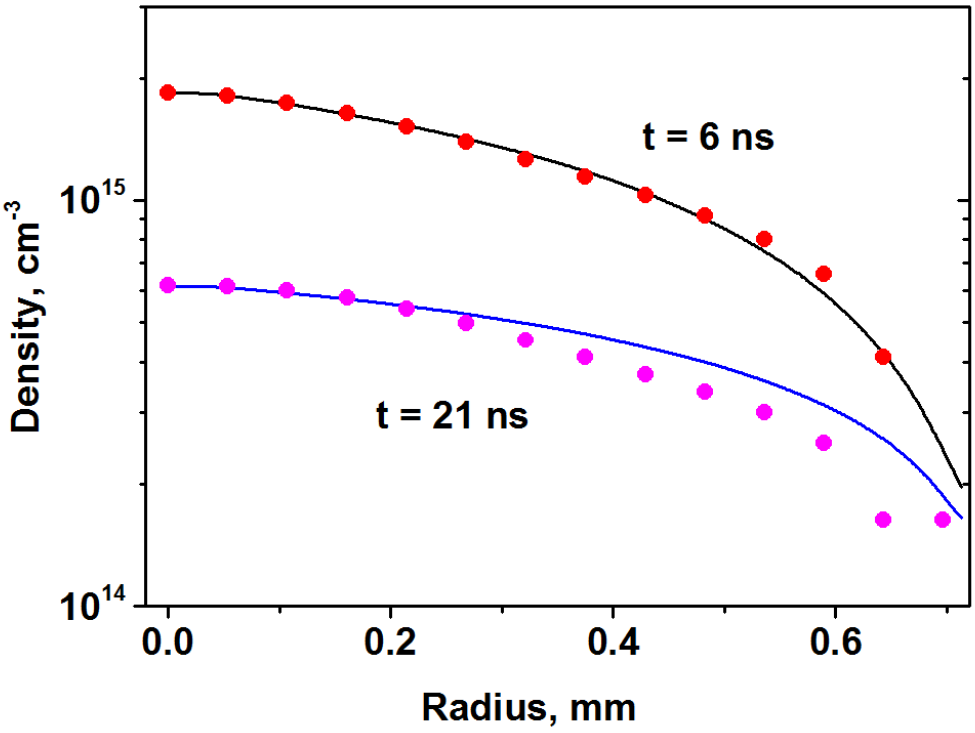

Figure 7. Radial profiles of electron density in the first pulse (t = 6 ns and 21 ns). Curves - calculations, points - the data derived from the emission of $N_2(C^3\Pi_u)$.

4.3. Derivation of radial profile of the electron density from the radial profile of the $N_2(C^3\Pi_u)$ *emission*

It has been discussed already that the correct description of radial profiles of the electron density in each of three pulses is an issue of a great importance. This is the radial distribution of the n_e which defines the values of specific deposited energy, density of atomic species and fast gas heating degree in the axial part of the discharge. To recall, the radial distribution of the intensity of $N_2(C^3\Pi_u)$ was studied experimentally and it can be related to the electron density provided that the (i) $N_2(C^3\Pi_u)$ state is mostly populated from the $N_2(X^1\Sigma_g^+)$ ground state, and (ii) the quenching rate of $N_2(C^3\Pi_u)$ should be independent on the radial coordinate. It has been previously shown that both conditions are fulfilled. Thereby, it is possible to derive the absolute values of the electron density as a function of radius of the capillary using the values of the electron density (see Table 1) measured in the pulses as a reference.

The Figures 7 and 8 demonstrate the radial profiles of the densities of charged species in the first pulse (t = 6 ns and 21 ns) and in the beginning of the second pulse (t = 241 ns). The points designate the measurements of the intensity of the SPS in CO_2:N_2 = 10:1 mixture. The initial distribution of the charged species in the first

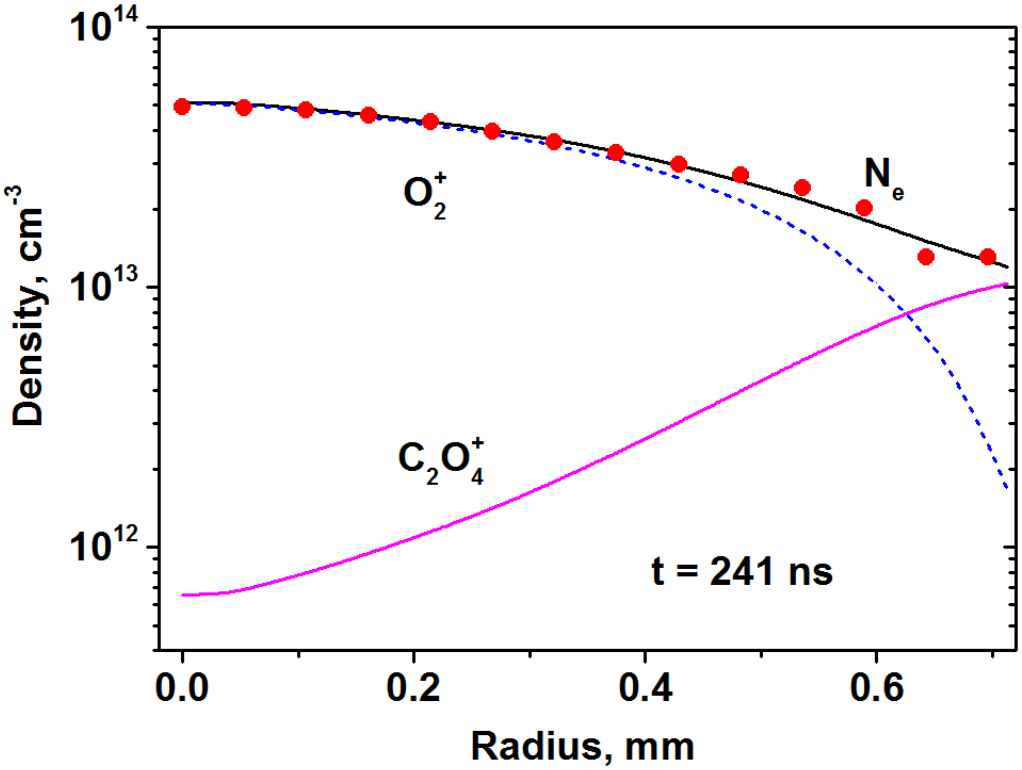

Figure 8. Radial profiles of electron density and positive ions before the second pulse (t = 241 ns). Curves - calculations, points - electron density derived from the measurements of the radial distribution of the $N_2(C^3\Pi_u)$ emission.

pulse has been taken according to the experimental data. It can be concluded from the results of numerical modeling that a pronounced maximum of the electron density on the tube axis is maintaining both in the second and third pulses whereas the electron-ion recombination should have made the distributions of charged species uniform in between the pulses. The explanation to this fact is the following. At $p = 19.4$ mbar and $T = 300$ K the frequency of formation of $C_2O_4^+$ ion in the reaction (R17):

$$CO_2^+ + CO_2 + M \longrightarrow C_2O_4^+ + M \qquad \text{(R17)}$$

is equal to $\nu_{17} = 7 \cdot 10^7$ s^{-1}. The increase of gas temperature causes a noticeable decrease of the rate of the reaction (R17). As the radial profile of electron density is 'contracted' towards the axial part of the capillary, the specific deposited energy and density of O-atoms is higher in the axial part as well. As a result, CO_2^+ ions are converged into O_2^+ during the reaction (R15):

$$CO_2^+ + O(^3P) \longrightarrow O_2^+ + CO \qquad \text{(R15)}$$

which is the most effective at the discharge axis. The rate of electron-ion recombination is almost 10 times lower for O_2^+ ion than for $C_2O_4^+$ ion [47]. Therefore, the recombination

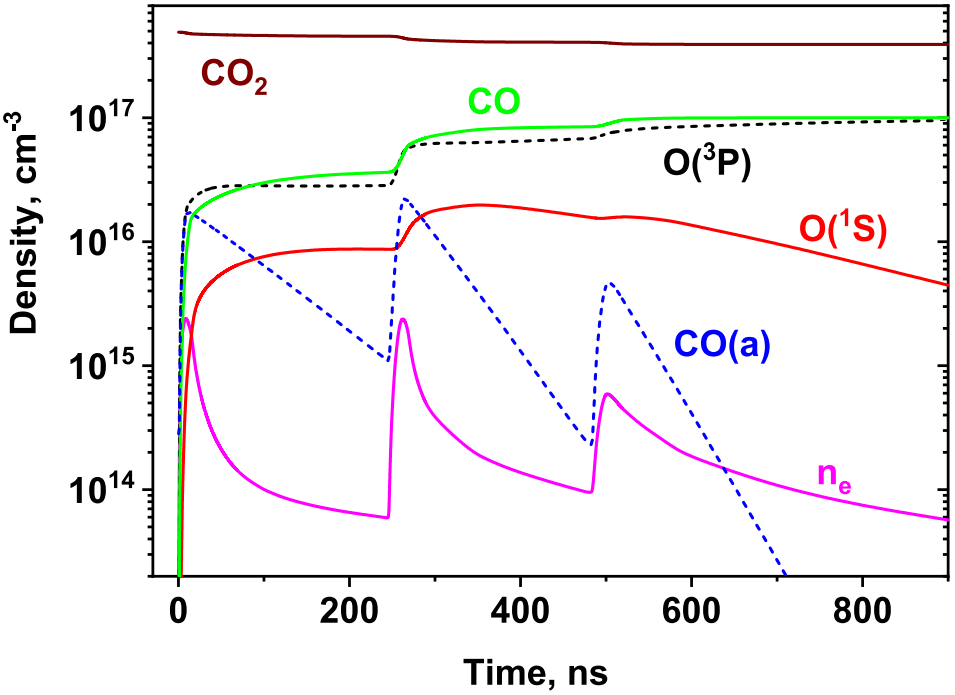

Figure 9. Calculations of the temporal dynamics of the species at the discharge axis. Pure CO_2, $p = 19.4$ mbar, initial gas temperature is $T_0 = 300$ K.

of electrons at the axial part, where O_2^+ ions dominate, is significantly lower than in the periphery of the discharge with dominance of $C_2O_4^+$ ions. This is the fact which explains the 'contraction' of the discharge to the axis. It should be noted that a similar 'memory effect' (reproduction of the electron density profile and its main features observed in the first pulse) was also observed in a capillary discharge in nitrogen [24]. In contrast, in nitrogen this effect was due to the reactions of associative ionization which provided additional production of charged particles in between high voltage pulses in regions with a high values of specific deposited energy (and high densities of excited $N_2(A^3\Sigma_u^+)$ and $N_2(a^1\Pi_g)$ molecules).

4.4. CO_2 dissociation and fast gas heating

Figure 9 shows the results of calculations of temporal dynamics of electron density n_e, oxygen atoms $O(^3P)$ and $O(^1S)$, molecules of CO and $CO(a^3\Pi)$ at the axis of the discharge in pure CO_2 at $p = 19.4$ mbar, $T_0 = 300$ K. The dissociation degree of CO_2 reached $\alpha \approx 20$ % at the discharge axis after the train of three pulses. Will note that the characteristic time of three-body recombination of CO and O at $T = 600 - 1500$ K is equal to $10 - 100$ ms, what is much higher than the characteristic times of the processes described in the present work. The energy efficiency of CO formation reached $G_{CO} = 8.5$ CO molecules/100 eV of deposited energy. This value is just 1.5 times lower than the G-value of production of atomic oxygen in the air at $E/n = 150$ - 250 Td [54, 55].

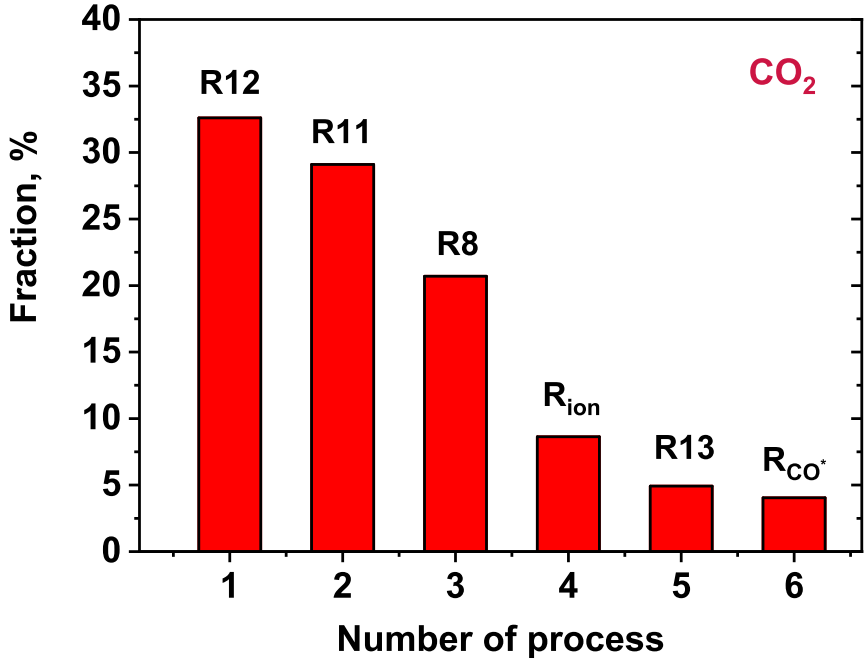

Figure 10. Distribution of energy release in fast gas heating between different processes near the discharge axis: 1 — quenching of $O(^1D)$ by CO_2 — reaction (R12); 2 — quenching of $O(^1S)$ by $O(^3P)$ — reaction (R11); 3 — quenching of $CO(a^3\Pi)$ by $O(^3P)$ — reaction (R8); 4 — reactions involving the charged particles R_{ion} = (R14)-(R16), (R19); 5 — quenching of $O(^1D)$ by CO — reaction (R13); 6 — quenching of $CO(a^3\Pi)$ by CO_2 and CO — reactions R_{CO*}= (R5)-(R7).

It should be mentioned that electronically excited species $CO(a^3\Pi)$ are actively produced in reactions of dissociation of CO_2 by electron impact (R3):

$$CO_2 + e \longrightarrow CO(a^3\Pi) + O(^3P) + e, \qquad \text{(R3)}$$

followed by fast quenching of $CO(a^3\Pi)$ by CO_2, CO and $O(^3P)$ (reactions (R5), (R6), (R7) and (R8)). It is assumed that quenching of $CO(a^3\Pi)$ by $O(^3P)$ atoms leads to formation of electronically excited $O(^1S)$ atoms which are followed by fast gas heating. The role of the reactions (R8), (R11)-(R13), (R14), (R16) and (R19) is demonstrated in Figure 10. It can be seen that the main origin of FGH at the given conditions is heat generation in the reactions of quenching of excited states of atomic oxygen and $CO(a^3\Pi)$:

$$O(^1D) + CO \longrightarrow O(^3P) + CO(v). \qquad \text{(R13)}$$

$$O(^1D) + CO_2 \longrightarrow O(^3P) + CO_2(v) \qquad \text{(R12)}$$

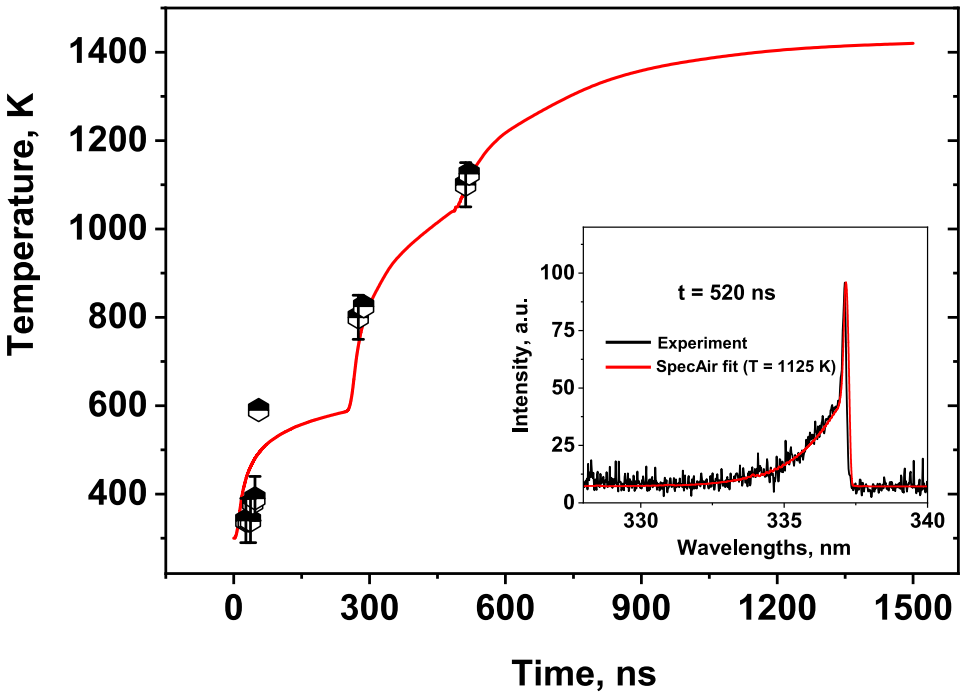

Figure 11. Temporal dynamics of gas temperature in three consequent pulses. The curve designates the calculation results, points designate experimental data. The fraction of energy coming to gas heating up to 2 μs is $\eta_R = 23$ %. The insert shows OES signal taken experimentally and the SpecAir fit.

$$O(^1S) + O(^3P) \longrightarrow O(^1D) + O(^3P) \quad \text{(R11)}$$

$$CO(a^3\Pi) + O(^3P) \longrightarrow CO(v) + O(^1S) \quad \text{(R8)}$$

$$CO(a^3\Pi) + CO_2 \longrightarrow CO(v) + CO_2(v) \quad \text{(R6)}$$

Figure 11 represents the temporal dynamics of gas temperature in three consequent pulses in the axial zone of the discharge. The curve designates the calculation results, the points are experimental data (in the model the dependence of heat capacity γ on gas temperature was taken from [56]). It can be seen that the model correctly describes the experimental data. The fraction of energy coming to the gas heating up to 2 μs is $\eta_R = 23$ % which is comparable to the efficiency of FGH at the same conditions in air and nitrogen [24]. It should be noted that the effect of gas heating in CO_2 plasma is significantly weaker than in N_2/air at approximately the same conditions. It is related to the fact that the adiabatic coefficient γ is significantly lower for CO_2 at 900-1500 K than for nitrogen (1.19 *vs* 1.33) [56].

5. Conclusions

Fast gas heating in pure CO_2 in a nanosecond capillary discharge at high values of specific deposited energy (around 1.2 eV/ molecule) and reduced electric fields (150–250 Td) has been studied experimentally and numerically at pressure p = 19-20 mbar. To measure the gas temperature, 10 % of N_2 molecules was added to CO_2 and rotational temperature of $N_2(C^3\Pi_u)$ was measured. The relation between the gas temperature and rotational temperature of $N_2(C^3\Pi_u)$ has been validated. A high increase of the gas temperature at sub-microsecond timescale has been observed by measurements: the gas temperature reached 1100 K during approximately 600 ns after the first high voltage pulse at the initial temperature of 300 K. A mechanism of fast gas heating at sub-microsecond timescale involving the reactions of quenching of $CO(a^3\Pi)$, $O(^1S)$ and $O(^1D)$ excited species has been suggested and validated by comparison of the experimental results and the results obtained by 1-D numerical modeling. The fraction of energy coming to the fast gas heating up to 2 μs is η_R = 23 %, which is comparable to the FGH efficiency observed in the approximately the same capillary discharge ignited in N_2 and air [31]. According to the calculations, $O(^1D)$ quenching by CO_2 molecules and $O(^1S)$ quenching by $O(^3P)$ atoms contribute the most (more than 50 %) in the gas heating.

The measurements of emission intensity of the second positive system of nitrogen in three high voltage pulses have shown that the emission intensity reaches the maximal value at the axis of the discharge and decreases monotonously towards the walls of the capillary. The relation between the radial profiles of the electron density and emission of $N_2(C^3\Pi_u)$ has been validated. The suggested explanation to the conservation of radial distribution of the electron density is based on a significant difference of ion composition at the discharge axis and the periphery. Active production of atomic oxygen at the discharge axis leads to the dominance of O_2^+ at the axis. The recombination rate of O_2^+ is significantly lower that the recombination rate of $C_2O_4^+$ ions which are dominant at the discharge periphery.

Acknowledgements

The work was partially supported by the French National Research Agency, ANR ('Atomic Species Production via Electronically excited states in high eNergy density Plasmas' (ASPEN) Project) and the French–Russian international Research Project KaPPA 'Kinetics and Physics of Pulsed Plasmas and their Afterglow'. The authors would like to thank Pascal Pariset for mechanical work. Helpful contributions from M. Haouchat Youssef and Dr. Orel Inna are also gratefully acknowledged.

References

[1] Fridman A A 2008 Plasma Chemistry. *Cambridge University Press*

[2] Rusanov V D, Fridman A A, Sholin G V 1981 The physics of a chemically active plasma with nonequilibrium vibrational excitation of molecules. *Sov. Phys. Usp.* **24** 447

[3] Legasov V A, Zhivotov V K, Krasheninnikov E G, Krotov M F, Patrushev B I, Rusanov V D, Rykunov G V, Spektor A M, Fridman A A and Sholin G V 1978 Nonequilibrium plasmochemical process of the decomposition in HF and SHF discharges. *Sov. Phys. Dokl.* **238** 66–69

[4] Snoeckx R and Bogaerts A 2017 Plasma technology – a novel solution for CO_2 conversion? *Chem Soc Rev* **46** 5805–5863

[5] Grofulović M, Alves L L and Guerra V 2016 Electron-neutral scattering cross sections for CO_2: a complete and consistent set and an assessment of dissociation *J. Phys. D: Appl. Phys.* **49** 395207

[6] Lowke J J, Phelps A V, Irwin B W 1973 Predicted electron transport coefficients and operating characteristics of CO_2–N_2–He laser mixtures. *Journal of Applied Physics* bf 44 4664

[7] Polak L S and Slovetsky D I 1976 Electron impact induced electronic excitation and molecular dissociation. *Int. J. Radiat. Phys. Chem.* bf 8 257-282

[8] Bogaerts A, Wang W, Berthelot A and Guerra V 2016 Modeling plasma-based CO_2 conversion: crucial role of the dissociation cross section. *Plasma Sources Science and Technology* **25** 055016

[9] Morillo-Candas A S, Silva T, Klarenaar B L M, Grofulović M, Guerra V and Guaitella O 2020 Electron impact dissociation of CO_2. *Plasma Sources Science and Technology* **29** 01LT01

[10] Babaeva N Yu and Naidis G V 2021 On the efficiency of CO_2 conversion in corona and dielectric-barrier discharges. *Plasma Sources Science and Technology* **30** 03LT03

[11] Silva T, Britun N, Godfroid T and Snyders R 2014 Optical characterization of a microwave pulsed discharge used for dissociation of CO_2. *Plasma Sources Science and Technology* **23** 025009

[12] Brehmer F, Welzel S, van de Sanden M C M, and Engeln R 2014 CO and byproduct formation during CO_2 reduction in dielectric barrier discharges. *J. Appl. Phys.* **116** 123303

[13] Klarenaar B L M, Engeln R, van den Bekerom D C M, van de Sanden M C M, Morillo-Candas A S and Guaitella O 2017 Time evolution of vibrational temperatures in a CO_2 glow discharge measured with infrared absorption spectroscopy. *Plasma Sources Science and Technology* **26** 115008

[14] Pietanza L D, Colonna G and Capitelli M 2020 Kinetics versus thermodynamics on CO_2 dissociation in high temperature microwave discharges. *Plasma Sources Science and Technology* **29** 035022

[15] Heijkers S, Martini L M, Dilecce G, Tosi P and Bogaerts A 2019 Nanosecond pulsed discharge for CO_2 conversion: kinetic modeling to elucidate the chemistry and improve the performance. *The Journal of Physical Chemistry* **123/19** 12104––12116

[16] Kozák T and Bogaerts A 2014 Splitting of CO_2 by vibrational excitation in non-equilibrium plasmas: a reaction kinetics model. *Plasma Sources Science and Technology* bf 23 045004

[17] Naidis G V and Babaeva N Yu 2021 Modeling of DC glow discharges in low-pressure CO_2. *Plasma Sources Science and Technology* **30** 105016

[18] Pietanza L D, Guaitella O, Aquilanti V, Armenise I, Bogaerts A, Capitelli M, Colonna G, Guerra V, Engeln R, Kustova E, Lombardi A, Palazzetti F and Silva T 2021 Advances in non-equilibrium CO_2 plasma kinetics: a theoretical and experimental review. *The European Physical Journal D - Atomic, Molecular and Optical Physics* **75** 237

[19] Martini L M, Lovascio S, Dilecce G and Tosi P 2018 Time-resolved CO_2 dissociation in a nanosecond pulsed discharge. *Plasma Chem Plasma Process* **38** 707—718

[20] Montesano C, Quercetti S, Martini L M, Dilecce G and Tosi P 2020 The effect of different pulse patterns on the plasma reduction of CO_2 for a nanosecond discharge. *Journal of CO_2 Utilization* **39** 101157

[21] Montesano C, Faedda M, Martini L M, Dilecce G and Tosi P 2021 CH_4 reforming with CO_2 in a nanosecond pulsed discharge. The importance of the pulse sequence. *Journal of CO_2 Utilization* **49** 101556

[22] Ceppelli M, Salden T P W, Martini L M, Dilecce G, Tosi P 2021 Time-resolved optical emission spectroscopy in CO_2 nanosecond pulsed discharges. *Plasma Sources Science and Technology* **30** 115010

[23] Klochko A V, Starikovskaia S M, Xiong Z and Kushner M J 2014 Investigation of capillary nanosecond discharges in air at moderate pressure: comparison of experiments and 2D numerical modelling. *J. Phys. D: Appl. Phys.* **47** 365202

[24] Lepikhin N D, Klochko A V, Popov N A and Starikovskaia S M 2016 Long-lived plasma and fast quenching of $N_2(C^3\Pi_u)$ by electrons in the afterglow of a nanosecond capillary discharge in nitrogen. *Plasma Sources Science and Technology* **25** 045003

[25] Klochko A V, L, emainque J, Booth J P and Starikovskaia S M 2015 TALIF measurements of oxygen atom density in the afterglow of a capillary nanosecond discharge. *Plasma Sources Science and Technology* **24** 025010.

[26] Klochko A V, Lemainque J, N A Popov, Booth J P and S M Starikovskaia 2013 Study of fast gas heating in a capillary nanosecond discharge in air. TALIF O

atoms measurements and kinetic modeling. *51st AIAA Aerospace Sciences Meeting including the New Horizons Forum and Aerospace Exposition*, 7-10 January, Grapevine, Texas, AIAA 2013-0574

[27] Chng T L, Lepikhin N D, Orel I S, Popov N A and Starikovskaia S M 2020 TALIF measurements of atomic nitrogen in the afterglow of a nanosecond capillary discharge. *Plasma Sources Science and Technology* **29** 035017

[28] Popov 2011 Fast gas heating in a nitrogen–oxygen discharge plasma: I. Kinetic mechanism. *Journal of Physics D: Applied Physics* **44** 285201

[29] Popov N A 2001 Investigation of the mechanism for rapid heating of nitrogen and air in gas discharges". *Plasma Phys. Rep.* **27** 886—896

[30] Rusterholtz D L, Lacoste D A, Stancu G D, Pai D Z and Laux C O 2013 Ultrafast heating and oxygen dissociation in atmo-spheric pressure air by nanosecond repetitively pulsed discharges. *Journal of Physics D: Applied Physics* **46** 464010

[31] Lepikhin N D, Popov N A and Starikovskaia S M 2018 Fast gas heating and radial distribution of active species in nanosecond capillary discharge in pure nitrogen and N_2:O_2 mixtures. *Plasma Sources Science and Technology* **27** 055005

[32] Anikin N B, Starikovskaia S M and Starikovskii A Yu 2004 Study of the oxidation of alkanes in their mixtures with oxygen and air under the action of a pulsed volume nanosecond discharge. *Plasma Physics Reports* 2004 **30** 1028—1042

[33] Bruggeman P J, Sadeghi N, Schram D C and Linss V 2014 Gas temperature determination from rotational lines in non-equilibrium plasmas: a review. *Plasma Sources Science and Technology* **23** 023001

[34] Laux C O, Spence T G, Kruger C H and Zare R N 2003 Optical diagnostics of atmospheric pressure air plasmas *Plasma Sources Sci. Technol.* **12** 125—138

[35] Albugues F, Birot A, Blanc D, Brunet H et al. 1974 Destruction of levels $C^3\Pi_u$ (v' = 0,1) of nitrogen by O_2, CO_2, CH_4, and H_2O. *Journal of Chemical Physics* **61(7)**, 2695-2699

[36] Hagelaar G J M and Pitchford L C 2005 Solving the Boltzmann equation to obtain electron transport coefficients and rate coefficients for fluid models. *Plasma Sources Science and Technology* **14** 722—733

[37] Slanger T, Black G, Fournier J 1975 Electronic-to-vibrational energy transfer between molecules *J. Photochem* **4** 329—339

[38] Piper L G 1982 The excitation of $O(^1S)$ in the reaction between $N_2(A^3\Sigma_u^+)$ and $O(^3P)$ *J. Chem. Phys.* **77** 2373—2377

[39] Radzig A and Smirnov B 1985 Reference Data on Atoms, Molecules and Ions *Springer, Berlin*

[40] Chen H-F, Chiang H-C, Matsui H, Tsuchiya S, Lee Y-P 2009 Distribution of vibrational states of CO_2 in the reaction $O(^1D)$ + CO_2 from time-resolved Fourier transform infrared emission spectra *J. Phys. Chem.* **113**, 3431—3437

[41] Slanger T and Black G 1974 Electronic-to-vibrational energy transfer efficiency in the $O(^1D)$–N_2 and $O(^1D)$–CO systems *J. Chem. Phys.* **60** 468—477.

[42] Silva A F, Morillo-Candás A S, Tejero-del-Caz A, Alves L L, Guaitella O and Guerra V 2020 A reaction mechanism for vibrationally-cold low-pressure CO_2 plasmas. *Plasma Sources Science and Technology* **29** 125020

[43] Schofield K 1979 Critically evaluated rate constants for gaseous reactions of several electronically excited species. *Journal of Physical and Chemical Reference Data* **8**, 723

[44] Smirnov B M 1982 Excited atoms. *Moscow, Energoizdat, 232 p. In Russian*

[45] Kossyi I A, Kostinsky A Y, Matveev A A, Silakov V P 1992 Kinetic scheme of the non-equilibrium discharge in nitrogen-oxygen mixtures. *Plasma Sources Science and Technology* **(3)** 207—220

[46] Dunlea E J, Ravishankara A R 2004 Kinetic studies of the reactions of $O(^1D)$ with several atmos-pheric molecules. *Phys. Chem. Chem. Phys.* **6** , 2152—2161

[47] Florescu A I, Mitchell J B A 2006 Dissociative recombination. *Physics Reports* **430** 277—374

[48] Mintoussov E I, Pendleton S J, Gerbault F G, Popov N A and Starikovskaia S M 2011 Fast gas heating in nitrogen–oxygen discharge plasma: II. Energy exchange in the afterglow of a volume nanosecond discharge at moderate pressures. *J. Phys. D: Appl. Phys.* **44** 285202

[49] Willis C, Boyd A W, Bindner P E 1970 Carbon monoxide yields in the radiolysis of carbon dioxide at very high dose rates. *Canadian Journal of Chemistry* **48** 1951—1954

[50] Park C 2004 Rotational relaxation of N_2 behind a strong shock wave. *Journal of Thermophysics and Heat Transfer* **18** 527—533

[51] Valentini P, Norman P, Zhang C and Schwartzentruber T E 2014 Rovibrational coupling in molecular nitrogen at high temperature: An atomic-level study *Physics of Fluids* **26** 056103

[52] Young R A, Black G and Slanger T G 1969 Vacuum-ultraviolet photolysis of N_2O. II Deactivation of $N_2(A^3\Sigma^+_u)$ and $N_2(B^3\Pi_g)$. *J. Chem. Phys.* **50** 303—308

[53] Phelps A V and Pitchford L C 1985 Anisotropic scattering of electrons by N_2 and its effect on electron transport. *Phys. Rev. A* **31**, 2932—2949

[54] Plank T, Jalakas A, Aints M, Paris P, Valk F, Viidebaum M and Jogi I 2014 Ozone generation efficiency as a function of electric field strength in air *J. Phys. D: Appl. Phys.* **47** 335205

[55] Popov N A 2016 Kinetics of plasma-assisted combustion: effect of non-equilibrium excitation on the ignition and oxidation of combustible mixtures. *Plasma Sources Sci. Technol.* **25** 043002

[56] Capitelli M, Colonna G and D'Angola A 2012 Fundamental Aspects of Plasma Chemical Physics.Thermodynamics, *Springer Series on Atomic, Optical and Plasma Physics, vol.66* Springer New York Dordrecht Heidelberg London